

## ORIGINAL RESEARCH

# Mitochondria-Rich Extracellular Vesicles Rescue Patient-Specific Cardiomyocytes From Doxorubicin Injury



## Insights Into the SENECA Trial

Connor G. O'Brien, MD,<sup>a,\*</sup> Mehmet Ozgun Ozen, PhD,<sup>b,c,\*</sup> Gentaro Ikeda, MD, PhD,<sup>b,d</sup> Evgeniya Vaskova, PhD,<sup>b,d</sup> Ji Hye Jung, PhD,<sup>b,d</sup> Nathan Bayardo, BA,<sup>b,d</sup> Michelle Rai Santoso, BA,<sup>b,d</sup> Liye Shi, MD, PhD,<sup>e</sup> Christine Wahlquist, PhD,<sup>b,d</sup> Zewen Jiang, BA,<sup>f,g</sup> Yunshin Jung, PhD,<sup>f,g</sup> Yitian Zeng, BA,<sup>h</sup> Elizabeth Egan, MD, PhD,<sup>i</sup> Robert Sinclair, PhD,<sup>h</sup> Adrian Gee, PhD,<sup>j</sup> Ronald Witteles, MD,<sup>d</sup> Mark Mercola, PhD,<sup>b,d</sup> Katrin J. Svensson, PhD,<sup>f,g</sup> Utkan Demirci, PhD,<sup>b,c,k</sup> Phillip C. Yang, MD<sup>b,d</sup>

### ABSTRACT

**BACKGROUND** Anthracycline-induced cardiomyopathy (AIC) is a significant source of morbidity and mortality in cancer survivors. The role of mesenchymal stem cells (MSCs) in treating AIC was evaluated in the SENECA trial, a Phase 1 National Heart, Lung, and Blood Institute-sponsored study, but the mechanisms underpinning efficacy in human tissue need clarification.

**OBJECTIVES** The purpose of this study was to perform an in vitro clinical trial evaluating the efficacy and putative mechanisms of SENECA trial-specific MSCs in treating doxorubicin (DOX) injury, using patient-specific induced pluripotent stem cell-derived cardiomyocytes (iCMs) generated from SENECA patients.

**METHODS** Patient-specific iCMs were injured with 1  $\mu\text{mol/L}$  DOX for 24 hours, treated with extracellular vesicles (EVs) from MSCs by either coculture or direct incubation and then assessed for viability and markers of improved cellular physiology. MSC-derived EVs were separated into large extracellular vesicles (L-EVs) (>200 nm) and small EVs (<220nm) using a novel filtration system.

**RESULTS** iCMs cocultured with MSCs in a transwell system demonstrated improved iCM viability and attenuated apoptosis. L-EVs but not small EVs recapitulated this therapeutic effect. L-EVs were found to be enriched in mitochondria, which were shown to be taken up by iCMs. iCMs treated with L-EVs demonstrated improved contractility, reactive oxygen species production, ATP production, and mitochondrial biogenesis. Inhibiting L-EV mitochondrial function with 1-methyl-4-phenylpyridinium attenuated efficacy.

**CONCLUSIONS** L-EV-mediated mitochondrial transfer mitigates DOX injury in patient-specific iCMs. Although SENECA was not designed to test MSC efficacy, consistent tendencies toward a positive effect were observed across endpoints. Our results suggest a mechanism by which MSCs may improve cardiovascular performance in AIC independent of regeneration, which could inform future trial design evaluating the therapeutic potential of MSCs.

(*J Am Coll Cardiol CardioOnc* 2021;3:428–440) © 2021 The Authors. Published by Elsevier on behalf of the American College of Cardiology Foundation. This is an open access article under the CC BY-NC-ND license (<http://creativecommons.org/licenses/by-nc-nd/4.0/>).

**A**nthracycline-induced cardiomyopathy (AIC) is one of the most morbid complications of chemotherapy (1). AIC is associated with a higher relative risk of death than both idiopathic and ischemic cardiomyopathy (2). Doxorubicin (DOX) enters the myocardium by passive diffusion (3), accumulating in the nucleus and mitochondria (4). Myocardial toxicity occurs via numerous mechanisms: 1) direct production of reactive oxygen species (ROS) and peroxide radicals by the quinone forms of anthracyclines (5); 2) ROS production mediated through iron-anthracycline complex redox reactions (6); and 3) topoisomerase 2B interactions leading to double-stranded DNA breaks (7). All lead to mitochondrial dysfunction and induction of apoptosis (8,9). DOX-induced ROS and double-stranded DNA breaks lead to nuclear translocation of ERK1/2 and p53, resulting in cytochrome C release driving collapse of mitochondrial membrane potential and apoptosis (8).

Stem cells have been evaluated as a reparative strategy. Despite poor cell retention (10), studies demonstrate that bone marrow-derived mesenchymal stem cells (MSCs) possess the ability to both prevent and reverse DOX-induced myocardial injury and fibrosis (11,12) as well as modulate neurohormonal systems active in heart failure (13). Therapeutic efficacy may be mediated through mitochondrial transfer (14).

Herein, we describe an in vitro clinical trial evaluating MSC-derived paracrine factors for efficacy in treating AIC in human cardiac tissue. We leveraged our participation in the National Institutes of Health/National Heart, Lung, and Blood Institute-sponsored SENECA trial (Phase I, First-in-Human, Multicenter, Randomized, Double-Blinded, Placebo-Controlled Study of the Safety and Efficacy of Allogeneic

Mesenchymal Stem Cells in Cancer Survivors with Anthracycline-Induced Cardiomyopathy). We successfully reprogrammed 3 patients' peripheral blood mononuclear cells into induced pluripotent stem cells (iPSCs) and differentiated these into cardiomyocytes (iCMs). Using these AIC patient-specific iCMs, we demonstrated that coculture of trial-specific MSCs successfully preserved iCM viability following DOX injury. We showed that this effect is mediated in a paracrine fashion via direct transfer of mesenchymal stem cell-derived extracellular vesicles (MSC-EVs) containing viable mitochondria. DOX-injured iCMs treated with MSC-EVs demonstrated reduced apoptosis, decreased ROS production, augmented ATP production, and preserved cellular physiology providing mechanistic insights into the results of the SENECA trial.

## METHODS

Detailed methods can be found in the [Supplemental Appendix](#).

**GENERATION OF PATIENT-SPECIFIC iPSCs.** We recruited 3 SENECA trial patients. This study was approved by Stanford University School of Medicine institutional review board committee (approval number: 35266). Patients were breast cancer survivors who were cancer free for  $\geq 2$  years, received  $>240$  mg/m<sup>2</sup> of DOX, and had a left ventricular ejection fraction  $<45\%$ . Peripheral blood mononuclear cells (PBMCs) were isolated, reprogrammed, and differentiated as described previously (9,15) ([Figure 1A](#), [Supplemental Figure 1](#)).

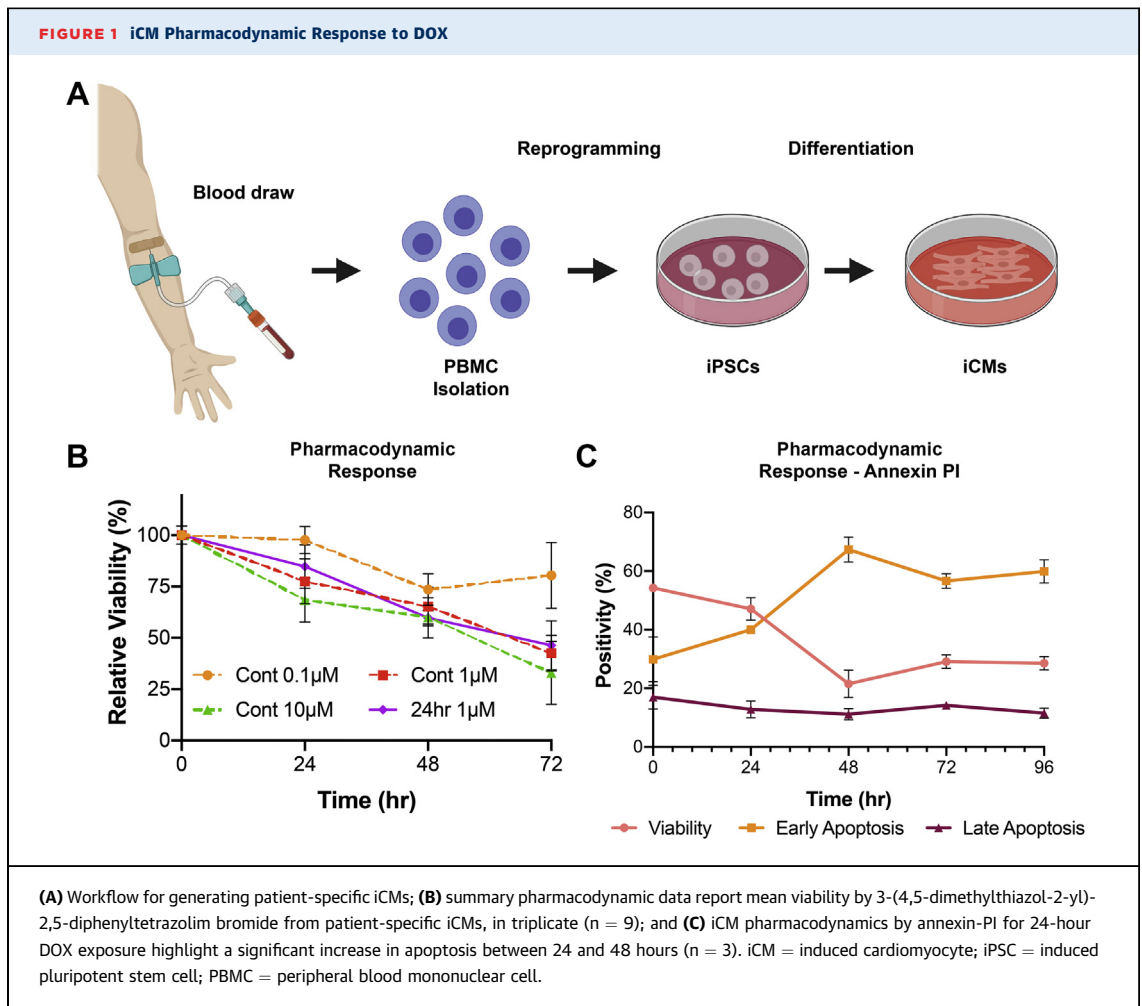
## ABBREVIATIONS AND ACRONYMS

<b>AIC</b>	= anthracycline induced cardiomyopathy
<b>DOX</b>	= doxorubicin
<b>DZR</b>	= dexrazoxane
<b>EV</b>	= extracellular vesicle
<b>iCM</b>	= induced cardiomyocyte
<b>L-EV</b>	= large extracellular vesicle
<b>MPP<sup>+</sup></b>	= 1-methyl-4-phenylpyridinium
<b>MSC</b>	= mesenchymal stem cell
<b>MSC-EV</b>	= mesenchymal stem cell derived extracellular vesicle
<b>MTDR</b>	= MitoTracker Deep Red
<b>MTG</b>	= MitoTracker Green
<b>RBC</b>	= red blood cell
<b>ROS</b>	= reactive oxygen species
<b>S-EV</b>	= small extracellular vesicle

From the <sup>a</sup>Department of Medicine, Division of Cardiology, University California San Francisco School of Medicine, San Francisco, California, USA; <sup>b</sup>Stanford Cardiovascular Institute, Stanford University School of Medicine, Stanford, California, USA; <sup>c</sup>Bio-Acoustic MEMS in Medicine BAMB Laboratory, Canary Center at Stanford for Cancer Early Detection, Department of Radiology, Stanford School of Medicine, Stanford University, Palo Alto, California, USA; <sup>d</sup>Department of Medicine, Division of Cardiovascular Medicine, Stanford University School of Medicine, Stanford, California, USA; <sup>e</sup>Department of Geriatric Cardiovascular Medicine, First Hospital of China Medical University, Shenyang, Liaoning, China; <sup>f</sup>Department of Pathology, Stanford University School of Medicine, Stanford, California, USA; <sup>g</sup>Stanford Diabetes Research Center, Stanford University School of Medicine, Stanford, California, USA; <sup>h</sup>Department of Materials Science and Engineering, Stanford University, Stanford, California, USA; <sup>i</sup>Department of Pediatrics (Infectious Diseases), Stanford University School of Medicine, Stanford, California, USA; <sup>j</sup>Center for Cell and Gene Therapy, Baylor College of Medicine, Texas Children's Hospital, Houston, Texas, USA; and the <sup>k</sup>Department of Electrical Engineering (by courtesy), Stanford, California, USA. \*Drs O'Brien and Ozen contributed equally to this work.

Lior Gepstein, MD, PhD, served as Guest Associate Editor for this paper. Anju Nohria, MD, served as Guest Editor-in-Chief for this paper.

The authors attest they are in compliance with human studies committees and animal welfare regulations of the authors' institutions and Food and Drug Administration guidelines, including patient consent where appropriate. For more information, visit the [Author Center](#).



### MSC-EV ISOLATION AND CHARACTERIZATION.

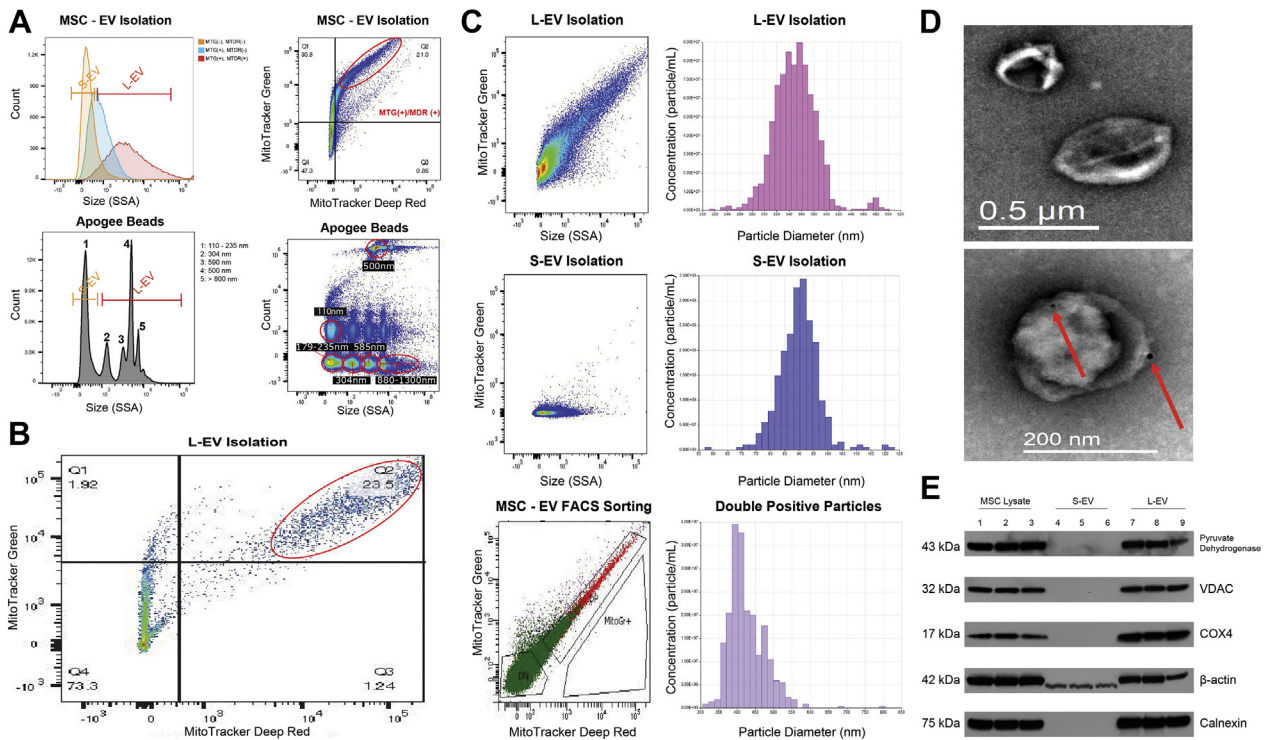
**Extracellular vesicle isolation and segregation.** MSCs were washed with phosphate-buffered saline (PBS) and Dulbecco's Modified Eagle Medium containing 10% exosome-free fetal bovine serum (Systems Biosciences) was added to culture. After 48 hours, MSC supernatant was centrifuged at 500g for 10 minutes and then isolated. Supernatant was either left unfiltered to isolate MSC-EV or passed through a 220 nm filter to isolate small extracellular vesicles (S-EV) as previously described (16). Extracellular vesicles (EVs) larger than 200 nmol/L (large extracellular vesicles [L-EVs]) were isolated using a proprietary size-based filtration platform named ExoTIC (Supplemental Figure 2) (17). MSC supernatant was centrifuged at 500g for 10 minutes then flowed through ExoTIC via syringe pump at 4°C. ExoTIC was decorated using a track-etched polycarbonate, low-protein binding filter with 200-nm pores concentrating L-EVs. L-EVs were eluted

from the filter with PBS. EVs were characterized using nanoparticle tracking analysis, flow cytometry (Supplemental Figure 3), western gel, and transmission electron microscopy (TEM) (Figure 2), as described in the Supplemental Methods and previously (18). Red blood cell (RBC)-derived L-EVs were isolated from supernatant collected from RBC cultures maintained in exosome-free conditions.

**Mitochondrial labeling.** MSC supernatant was collected as described in the previous text and was stained with 50 nmol/L MitoTracker Green™ (MTG) and/or MitoTracker Deep Red™ (MTDR) (Thermo Fisher Scientific). EVs were then isolated and washed as described previously for analysis by flow cytometry.

**DOXORUBICIN EXPOSURE ASSAYS. In vitro anthracycline induced cardiomyopathy model.** iCMs were seeded on 12-well plates ( $2.5 \times 10^5$  iCMs/well). For iCMs treated with dexrazoxane (DZR), 100 µmol/L dexrazoxane in iCM maintenance media was added 2

**FIGURE 2 EV Size and Mitochondrial Content Characterization**



(A, top left) Representative dot plot of MSC-EVs displaying a population of MitoTracker Green positive [MTG(+)] and MitoTracker Deep Red positive [MTDR(+)] EVs in the L-EV (>200 nm) size range by side scatter. (A, top right) Dot plot of the same MSC-EVs in top left gated to show MTG(+)/MTDR(+) vesicles (red oval). (A, bottom) Apogee bead reference dot plot (right) and size histogram (left). (B) Representative dot plot for L-EVs showing a distinct MTG(+)/MTDR(+) population (red oval). (C, top) Representative dot plot for L-EVs with accompanying qNano analysis demonstrated a mean particle size of 352 nm (216-498 nm). (C, middle) Representative dot plot for S-EVs showing smaller side scatter profile lacking MTG signal with accompanying qNano analysis showing mean particle size of 92 nm (58-122 nm). (C, bottom) Representative dot plot for BD FACSaria sorting of MSC-EVs showing relative size by side scatter of mitochondria(+) EVs (red) vs mitochondria(-) EVs (green) with accompanying qNano analysis of sorted mitochondria(+) EVs showing mean particle size of 428 nm (350-800 nm), similar to L-EVs. (D, top) TEM image of L-EVs measuring 250-500 nm. (D, bottom) Immunogold (10 nm) labeling showing 200-500 nm L-EVs are CD9(+) (red arrows) (n = 3). (E) Western blot confirming presence of complete mitochondria within L-EVs and MSC-lysate represented by outer membrane (VDAC), inner membrane (COX4), and matrix (pyruvate dehydrogenase) proteins (n = 3). COX4 = cytochrome C oxidase subunit 4; VDAC = voltage dependent anion channel; other abbreviations as in Figure 3.

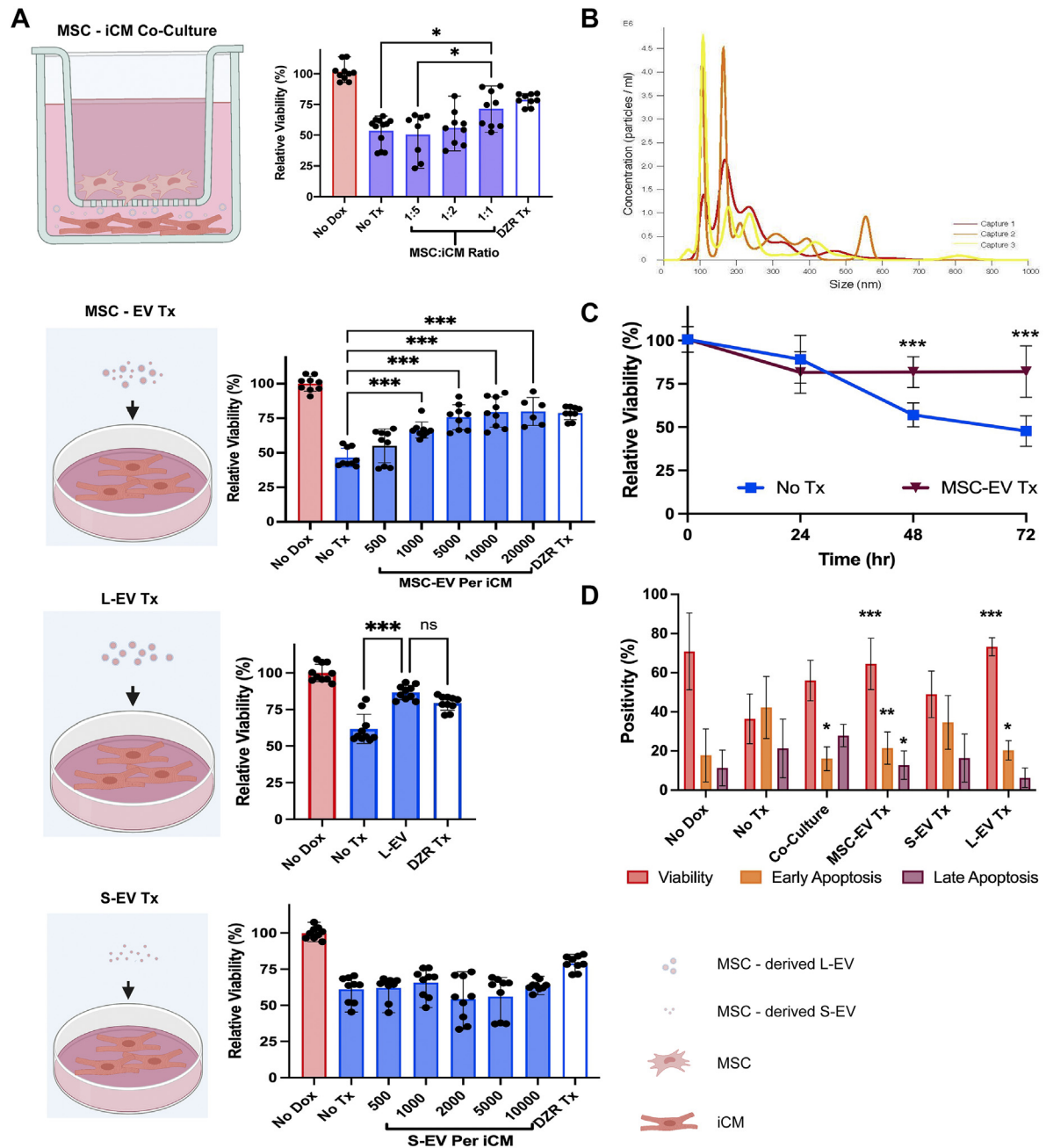
hours prior to DOX exposure. 0.1, 1, or 10  $\mu\text{mol/L}$  DOX in iCM maintenance media was added to culture for 24, 48, or 72 hours. All treatment assays adhered to a 1- $\mu\text{mol/L}$  exposure for 24 hours. Cells were washed and iCM maintenance medium with or without MSC-EV, S-EV, or L-EV was added to culture. Viability was then assessed by either 3-(4,5-dimethylthiazol-2-yl)-2,5-diphenyltetrazolium bromide or annexin-PI assay per manufacturer protocol.

**1-methyl-4-phenylpyridinium assays.** L-EVs were exposed to 10 mmol/L 1-methyl-4-phenylpyridinium (MPP+) for 90 minutes (19), centrifuged at 10,000g for 30 minutes, resuspended in 20 mL of MSC media, and collected using Exo-TIC. Loss of mitochondrial membrane potential was confirmed with JC-1 (Cayman Chemical) and MTG/MTDR staining

(Supplemental Figure 4), and 50  $\mu\text{mol/L}$  carbonyl cyanide m-chlorophenyl hydrazone served as a positive control.

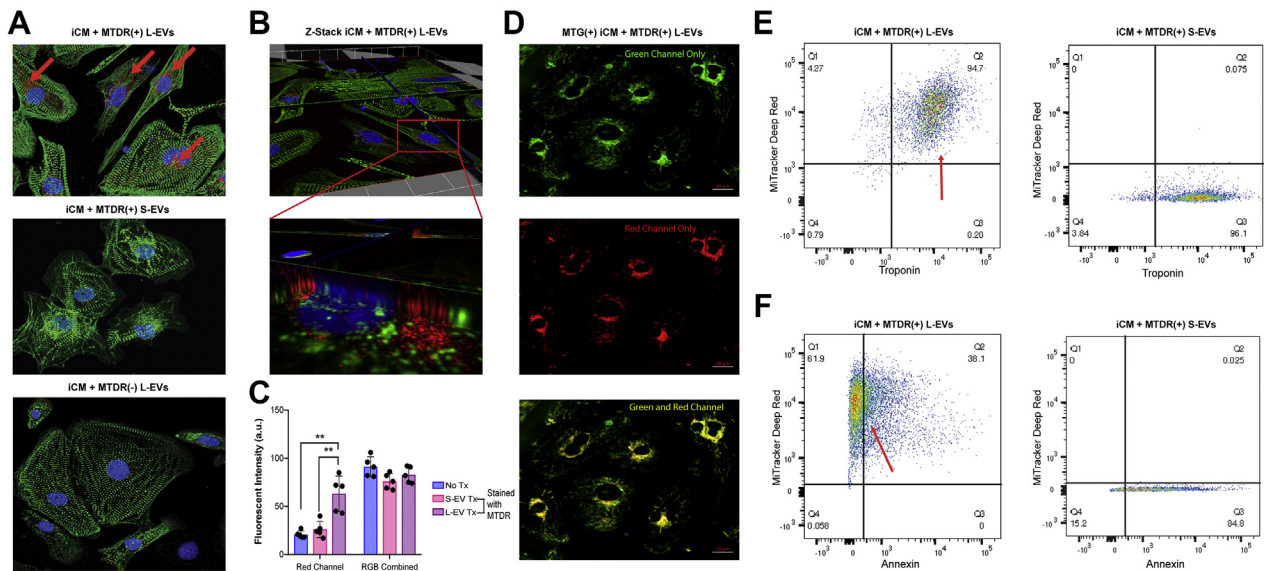
**Cell physiology assays.** The 96-well plates (Greiner Bio-One) were seeded with  $1 \times 10^5$  iCMs/well. iCMs were exposed to 1  $\mu\text{mol/L}$  DOX for 24 hours and then received iCM maintenance media either with or without S- or L-EV. iCM beating was confirmed prior to initiating analysis.

**Immunohistochemical analysis of L-EV uptake.** iCMs were seeded onto MatriGel (Corning) coated coverslips. S- and L-EVs were incubated in 50 nmol/L MTDR for 1 hour immediately before isolation as described in the previous text. A total of  $1 \times 10^8$  MTDR stained S- or L-EVs were added to iCM culture at 37°C for 6 hours. iCMs were washed, fixed, and stained as described

**FIGURE 3** Pharmacodynamic Effect of MSC Co-culture and Paracrine Therapy on DOX Injury

(A) 3-(4,5-dimethylthiazol-2-yl)-2,5-diphenyltetrazolium bromide 48-hour iCM viability assays showing: (Top) iCMs cocultured with MSCs demonstrated significant improvement in viability at a 1:1 culture ratio ( $n = 9$ ). (Second) MSC-EVs had a dose-dependent effect and an optimized therapeutic response at 5,000 EV/iCM ( $n = 9$ ). (Third) L-EVs significantly improved iCM viability similar to MSC-EV ( $n = 9$ ). (Fourth) S-EVs did not mitigate DOX-induced cell death ( $n = 9$ ). DZR treatment served as a positive control in all assays showing preservation of iCM viability. (B) Nanoparticle tracking analysis of MSC-EVs highlights distinct S- and L-EV populations ranging from 90-800 nm; (C) 3-(4,5-dimethylthiazol-2-yl)-2,5-diphenyltetrazolium bromide 72-hour viability assay demonstrated sustained therapeutic effect of MSC-EVs. (D) AnnexinV-PI data showed reduced apoptosis and improved viability at 48 hours following MSC coculture, MSC-EV, and L-EV treatments, but no response to S-EVs ( $n = 9$ ). All viability assays were performed in 3 patient lines in triplicate. \* $P < 0.05$ , \*\* $P < 0.01$ , and \*\*\* $P < 0.001$  by a 1-way analysis of variance or 2-way analysis of variance with repeated measures followed by Tukey's test. DZR = dexrazoxane; EV = extracellular vesicle; iCM = induced cardiomyocyte; L-EV = large extracellular vesicle; MSC = mesenchymal stem cell; MSC-EV = mesenchymal stem cell derived extracellular vesicle; S-EV = small extracellular vesicle.

**FIGURE 4** Mitochondria From L-EVs Are Directly Taken Up by iCMs



(A, top) iCMs incubated with MTDR-stained L-EVs (red) demonstrated colocalized MTDR signal (red arrows) and alpha-actin (green). (A, middle and bottom) iCMs incubated with MTDR-stained S-EVs or unstained L-EVs, respectively, demonstrated an absence of MTDR signal (n = 6). (B, top) z-stack analysis of same visual field from A, top demonstrated an intracytoplasmic and perinuclear MTDR signal. (B, bottom) Magnified view of a single iCM (red box). (C) ImageJ quantification showing MTDR(+) L-EV-treated iCMs demonstrated increased red channel signal intensity compared with iCMs treated with MTDR(+) S-EVs and untreated. P value <0.01 by 1-way analysis of variance followed by Tukey's test (n = 6). Combined Color Channel intensity did not differ across iCMs. (D) MTG-stained iCMs incubated with MTDR-stained L-EVs showed expected perinuclear distribution of native mitochondria (green) (top), MTDR uptake (red) (middle), and co-localization of MTG and MTDR signal (yellow) suggesting fusion of L-EV-derived and native iCM mitochondria (bottom). (E) Representative dot plots show cardiac troponin-T (cTnT)-labeled iCMs incubated with MTDR-stained L-EVs (left) with colocalization (red arrow), suggesting mitochondrial uptake, whereas iCMs incubated with MTDR-stained S-EVs (right) showed no colocalization (n = 3). (F) Representative dot plots show DOX-injured iCMs treated with MTDR-stained L-EVs (left) with reduced annexin V signal and greater MTDR uptake (red arrow) than iCMs treated with MTDR-stained S-EVs, suggesting mitochondrial-uptake correlates with reduced apoptosis. Abbreviations as in Figures 1 and 3.

previously (20). For colocalization experiments, iCMs were stained with 100 nmol/L MTG per protocol, washed, incubated with MTDR(+) L-EVs for 6 hours, washed, and imaged in PBS.

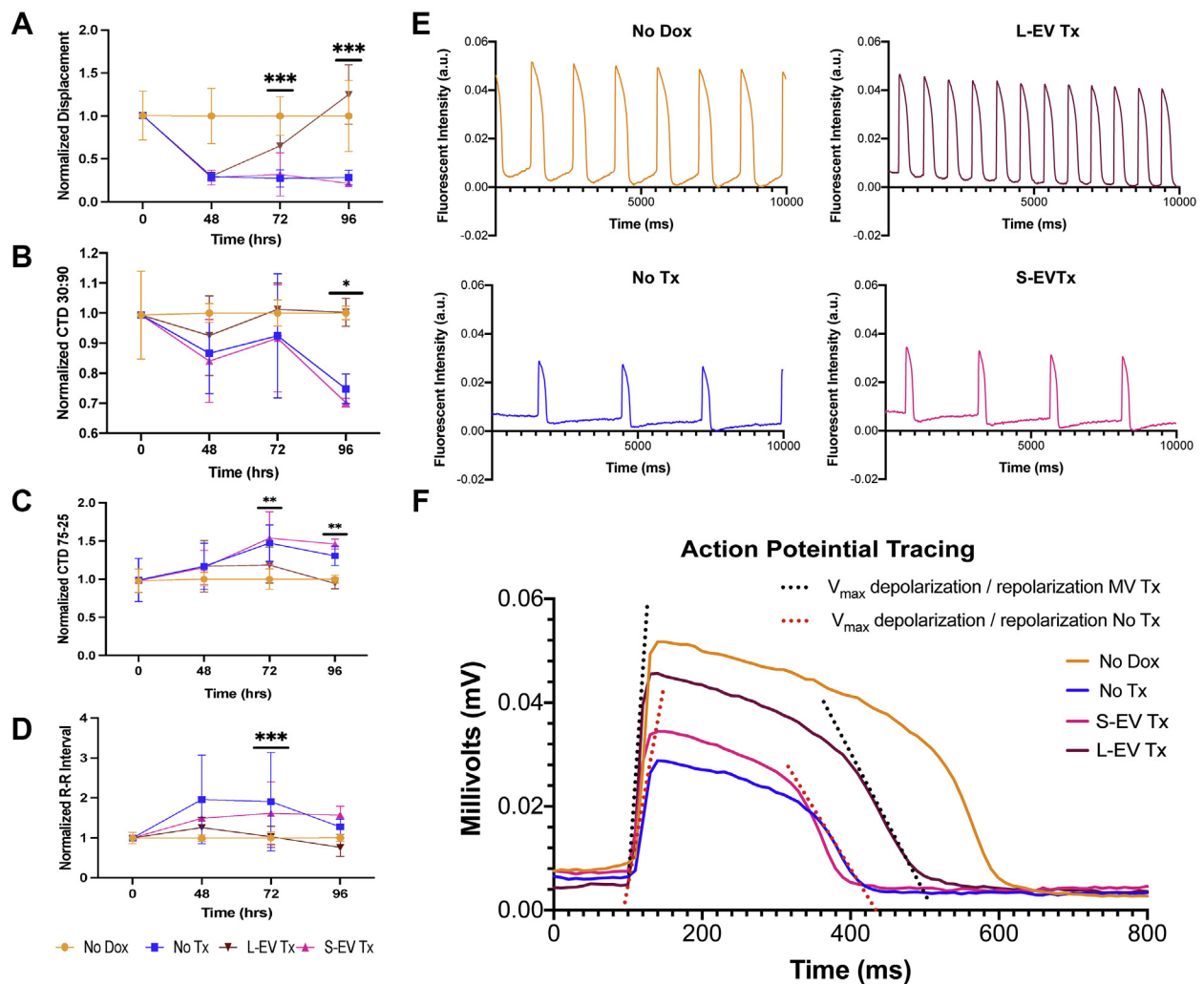
**STATISTICAL ANALYSIS.** Data are presented as mean ± SD. Statistical significance was determined by unpaired Student's *t*-tests for comparisons of 2 groups, 1-way analysis of variance followed by Tukey's post hoc Tukey test for multiple pairwise comparisons among 3 or more groups at a single time point, or 2-way analysis of variance with repeated measures for comparisons among 3 groups or more at multiple time points (Prism 8.3, GraphPad Software). A P value <0.05 was considered significant.

## RESULTS

**DOX PHARMACODYNAMICS IN iCMs.** Our patient-specific iCM lines demonstrated similar sensitivity to DOX when compared with previously published values in patient-specific lines (Figures 1B and 1C)

(9). Modern DOX protocols result in areas under the curve and C<sub>max</sub> of ~3.8 μmol/L·h and 1.65 μmol/L, respectively (21,22). In vitro, this converts to 1 μmol/L DOX exposure for 24 hours, which results in equal cell death at 24, 48, and 72 hours as continuous exposure protocols (Figure 1B). Using an annexin-PI assay, we demonstrated that the iCMs exposed to DOX for 24 hours underwent a dramatic increase in apoptosis 24-48 hours after DOX exposure (Figure 1C), suggesting that the majority of cardiomyocyte injury in vitro occurs in the first 24 hours of exposure. Based on this result, we chose to treat at 24 hours and evaluate survival and cellular function at 48 hours.

**CO-CULTURE WITH MSCs IMPROVES CARDIOMYOCYTE VIABILITY.** Using a 1,000 nm transwell system (Figure 3A), we demonstrated a dose-dependent improvement in viability following DOX exposure in iCMs cocultured with MSCs. Cardiomyocyte viability improved significantly in coculture when

**FIGURE 5** L-EVs Improve Cardiomyocyte Function After DOX Injury

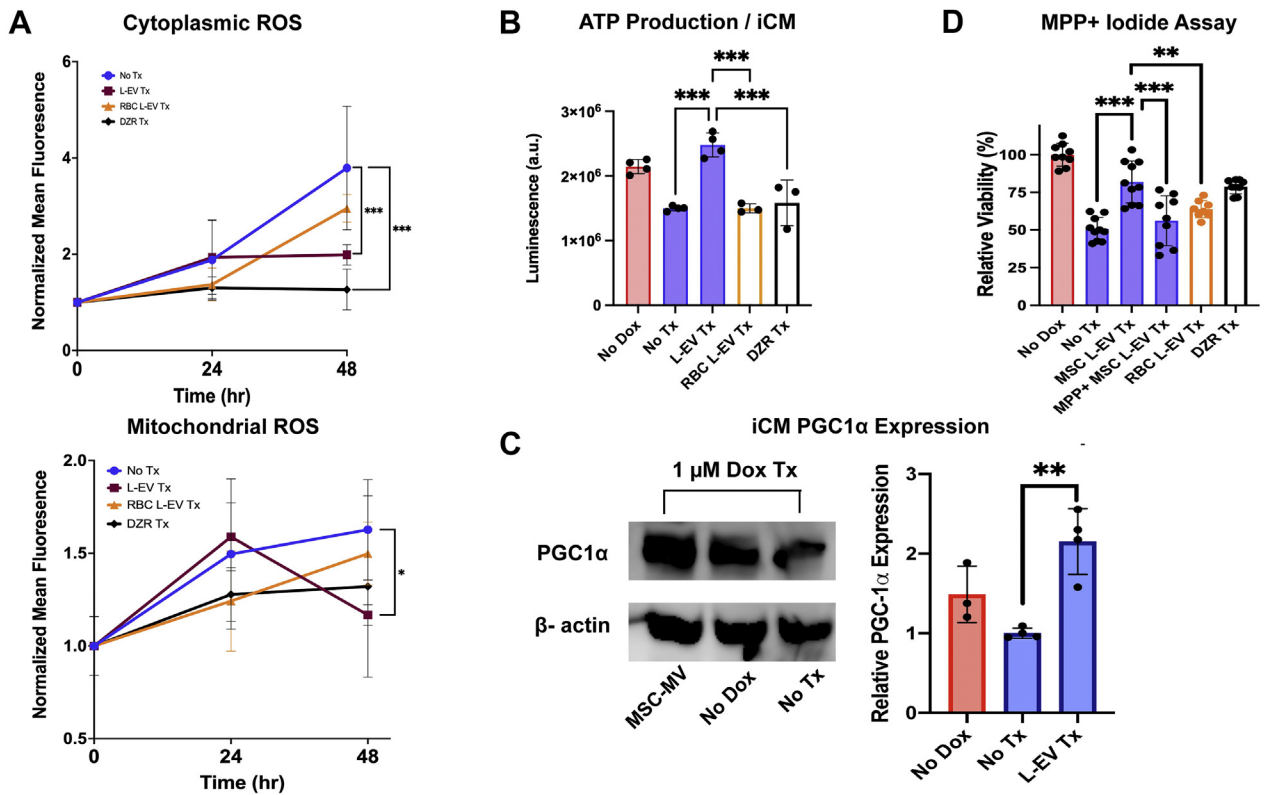
Asterisks indicate significant differences between No Tx and L-EV Tx groups by repeated measures, 2-way analysis of variance. \* $P < 0.05$ , \*\* $P < 0.01$ , \*\*\* $P < 0.001$ . **(A)** Peak membrane displacement (D-peak) showed recovery of iCM contractility in L-EV-treated iCMs ( $n = 20$ ). **(B and C)** Calcium transient duration (CTD) 30:90 and 75:35 showed significantly enhanced recovery speed of calcium release and sequestration during iCM contraction and active relaxation, respectively, in L-EV-treated iCMs ( $n = 20$ ). **(D)** Beat frequency recovered after DOX-injury in L-EV-treated iCMs but not in positive control subjects or S-EV-treated iCMs ( $n = 20$ ). **(E)** Representative calcium transient tracing from all 4 groups at 96 hours showed greater signal amplitude, faster upstroke, more rapid signal recovery, and higher beat frequency in DOX-injured iCMs treated with L-EVs compared with negative control and S-EV-treated iCMs ( $n = 5$ ). **(F)** Representative action potential (AP) tracing from iCMs at 96 hours showed recovery of AP amplitude, upstroke  $V_{max}$ , and downstroke  $V_{max}$  in DOX-injured iCMs treated with L-EVs relative to negative control subjects and S-EV-treated iCMs ( $n = 5$ ). Abbreviations as in [Figures 1 and 3](#).

iCMs and MSCs were cocultured in a 1:1 ratio, resulting in a 48% improvement in viability ( $P = 0.038$ ) ([Figure 3A](#)).

Given the absence of cell-cell contact within the transwell system, we hypothesized that the survival benefit must be mediated by paracrine factors. Nanoparticle tracking analysis of MSC-supernatant showed 2 populations of MSC-EVs that could transit through transwell pores: a population in the

exosome size range (30-200 nm) and a population in the microvesicle size range (200-800 nm) ([Figure 3B](#)). To test if MSC-EVs are responsible for the paracrine effects, MSC-EVs were added to iCM culture at day 1 following DOX exposure ([Figure 3A](#)). MSC-EVs improved iCM viability in a dose-dependent fashion ([Figure 3A](#)). Viability remained steady at 72 hours in MSC-EV-treated iCMs, whereas viability in untreated iCMs continued to

**FIGURE 6** Mitochondrial Transfer Reduces ROS, Augments ATP, and Preserves Mitochondrial Biogenesis



(A) iCMs treated with L-EVs at 24 hours following DOX injury showed reduced cytoplasmic (top, CellROX Deep Red) and mitochondrial (bottom, CellROX Green) ROS production (n = 6). (B) Following DOX injury, iCMs treated with L-EVs demonstrate greater ATP production per iCM (n = 4). (C, left) Representative western blot showing Peroxisome proliferator-activated receptor-gamma coactivator 1 (PGC1)-alpha expression in iCMs. (C, right) ImageJ analysis of relative PGC1-alpha expression in 3 iCM groups following DOX injury. iCMs treated with L-EVs show greater expression than both no DOX and DOX-injured iCMs (n = 4). (D) 3-(4,5-dimethylthiazol-2-yl)-2,5-diphenyltetrazolium bromide 48-hour viability assay showing MPP+ iodide attenuates the therapeutic effect of L-EVs. Red blood cell (RBC)-derived L-EVs lack mitochondria and show no therapeutic effect. Dexrazoxane (DZR) serves as positive control (n = 9). \*P < 0.05, \*\*P < 0.01, and \*\*\*P < 0.001 by 1-way analysis of variance or 2-way analysis of variance with repeated measures followed by Tukey's test. Abbreviations as in Figures 1 and 3.

decline (Figure 3C). MSC-EVs did not artificially amplify the 3-(4,5-dimethylthiazol-2-yl)-2,5-diphenyltetrazolium bromide signal (Supplemental Figure 5D). Treatment with 100 μmol/L DZR was used as a control therapy, showing consistent preservation of iCM viability.

**L-EVs IMPROVE iCM VIABILITY.** We separated MSC-EVs into S-EVs (<200 nm) and L-EVs (>200 nm). We tested each population separately. L-EVs significantly improved viability at 48 hours (P < 0.001) (Figure 3A). In contrast, S-EV demonstrated no effect on iCM viability across a broad dose range (P = 0.19) (Figure 3A). Flow cytometry analysis further supported a therapeutic effect showing that apoptosis was inhibited by L-EV, MSC-EV, and coculture, but not S-EV in an annexin-V assay (Figure 3D).

**L-EVs ARE ENRICHED WITH MITOCHONDRIA.** MSCs have been shown to mitigate anthracycline injury by donating mitochondria to injured cardiomyocytes via nanotubes (14). Guided by these findings, we analyzed MSC-EVs for mitochondrial content (Figure 2A). We identified 3 vesicle populations: 1) 110-235 nm size range and double negative for MTG and MTDR [MTG(-)/MTDR(-)]; 2) 200-400 nm size range and MTG(+)/MTDR(-), suggesting the presence of nonviable mitochondria or mitochondrial fragments; and 3) 300-800 nm size range and MTG(+)/MTDR(+), suggesting the presence of viable mitochondria. This MTG(+)/MTDR(+) population is enriched in L-EV (Figure 2B). We then sorted MTG(+)/MTDR(+) MSC-EVs (Figure 2C) using a FACSaria (Becton Dickinson). Using tunable resistive pulse

**TABLE SENECA Trial Findings of 3 Patients**

	Relative Change From Baseline at 12 Months		Average Absolute Change From Baseline at 12 Months	
	MSC Treated	Placebo Treated	MSC Treated	Placebo Treated
	(n = 1)	(n = 2)	(n = 1)	(n = 2)
Left ventricular ejection fraction	+19	+18 <sup>a</sup>	+7	+7 <sup>a</sup>
Global longitudinal strain	-15	+18	-1.84	+1.99
Left ventricular myocardial scar	-20	+64 <sup>a</sup>	-2.70	+3.86 <sup>a</sup>
6-min walk test	+18	+6	+68.5 feet	+18 feet
Minnesota living with heart failure questionnaire	-51	-7	-24.85 points	-5 points

Values are % unless otherwise indicated. The table reflects the relative percentage change from baseline achieved by 3 trial patients at 12 months of follow-up. <sup>a</sup>Incomplete 12-month data, n = 1.  
MSC = mesenchymal stem cell.

sensing (qNano, Izon, TRPS), we found this sorted population to be similar in size to L-EVs: mean size 352 nm (216-498 nm) vs 428 nm (350-800 nm), respectively (Figure 2C). S-EV isolations measured 58-122 nm with a mean size of 92 nm by TRPS (Figure 2C) and were consistently MTG(-)/MTDR(-) (Supplemental Figure 3B). We further characterized our L-EVs with TEM and Western blotting. Bright field TEM evaluation of L-EVs demonstrated CD9+ particles ranging from 220-500nm (Figure 2D). Western blot showed that L-EVs but not S-EVs were calnexin positive (Figure 2E). Our TEM and Western data suggest that L-EVs are microvesicles and S-EVs are exosomes (23), which is consistent with prior EV profiling work done in our laboratory (18,24). Western blot showed that L-EVs contain intact mitochondria by demonstrating presence of mitochondria-specific inner membrane, outer membrane, and matrix proteins (voltage dependent anion channel, cytochrome C oxidase subunit 4, and pyruvate dehydrogenase, respectively), which were absent in S-EV preparations (Figure 2E).

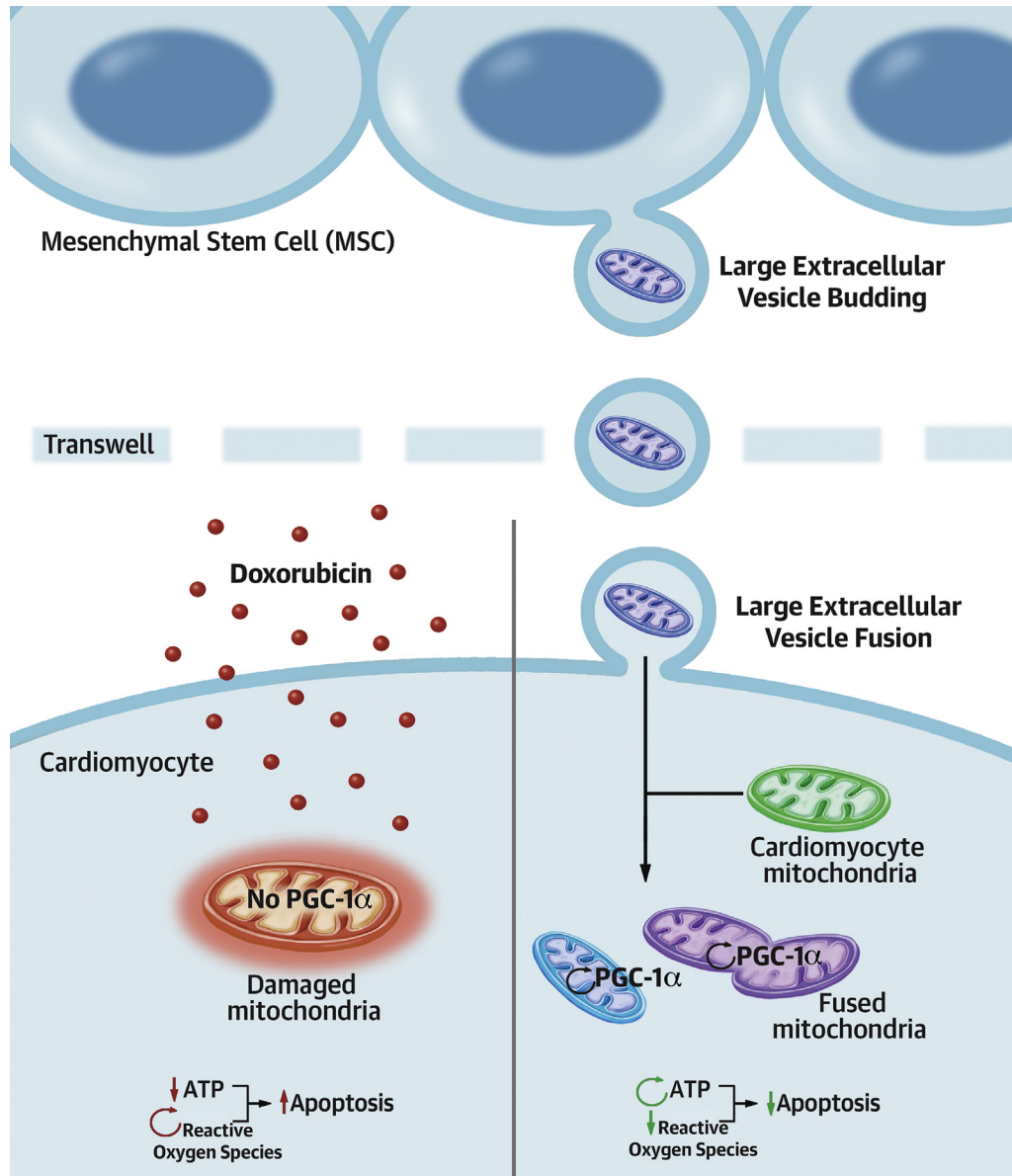
**L-EV MITOCHONDRIA ARE TAKEN UP BY PATIENT-SPECIFIC iCMs.** Using confocal microscopy and 3-dimensional analysis, iCMs incubated with MTDR(+) L-EVs were shown to accumulate MTDR signal within iCM cytoplasm (Figures 4A and 4B). iCMs incubated with MTDR-stained S-EVs showed no MTDR uptake (Figure 4B). ImageJ analysis shows higher maximal Red Channel signal confirming MTDR uptake ( $P = 0.004$ ) (Figure 4C). The MTDR signal consistently demonstrated a perinuclear distribution, which is the natural distribution of mitochondria in iCMs. Based on this observation, we stained native mitochondria with MTG and were able to show MTDR and MTG signal colocalization following MTDR(+) L-EV treatment, suggesting that the separate mitochondria undergo fusion (Figure 4D, Supplemental

Figure 6). iCM uptake of L-EVs was further demonstrated using flow cytometry. iCMs incubated with MTDR(+) L-EVs exhibit colocalized MTDR and troponin signal, whereas iCMs incubated with S-EVs showed no colocalization (Figure 4E). Furthermore, DOX-injured iCMs treated with MTDR(+) L-EVs demonstrated mitochondrial uptake and reduced annexin signal compared with S-EV-treated iCMs ( $P = 0.036$ ) (Figure 4E). Uptake of MSC L-EV mitochondria was robust because ~95% of iCMs demonstrated MTDR positivity after coincubation with MTDR(+) L-EVs (Figures 4E and 4F).

**L-EVs IMPROVE iCM PHYSIOLOGY.** Contractility, calcium transients, and electrophysiological properties of iCMs were evaluated. iCM contractility significantly improved following L-EV treatment. Peak contractility declined dramatically in all DOX-injured groups after DOX exposure (Figure 5A). Between 48 and 96 hours, L-EV- but not S-EV-treated iCMs recovered contractility (at 96 hours,  $P < 0.001$ ) (Figure 5A). Similarly, we demonstrated reduced calcium flux (calcium transient duration 30:90) and prolonged calcium decay (calcium transient duration 75:25) after DOX injury with near normalization between 72 and 96 hours in L-EV- but not S-EV-treated iCMs (Figures 5B and 5C, respectively). DOX injury depressed contractile rates, which normalized after L-EV treatment (Figure 5D). Figure 5E shows representative calcium transients tracings from each group demonstrating differences in signal amplitude and contractile frequency at 96 hours. DOX injury resulted in significant negative effects on iCM action potential, including depressed peak values, reduced  $V_{max}$  upstroke in phase 0, and reduced  $V_{max}$  downstroke in phase 3. Treatment with L-EVs but not S-EVs improved peak potential ( $P = 0.002$ ), upstroke  $V_{max}$  ( $P = 0.002$ ), and downstroke  $V_{max}$  ( $P = 0.027$ ) (Figure 5F). Rise and decay time were not significantly different because of decreased action potential amplitude in DOX-injured iCMs.

**L-EVs REDUCE ROS PRODUCTION AND PRESERVE MITOCHONDRIAL BIOGENESIS AND FUNCTION.** Treatment with L-EVs preserved mitochondrial function in iCMs. L-EVs attenuated both cytoplasmic and mitochondrial ROS production ( $P < 0.001$  and  $P = 0.030$ , respectively) (Figure 6A). Similarly, L-EV treatment augmented ATP production per iCM ( $P < 0.001$ ) (Figure 6B), a phenomenon also seen in our coculture experiments (Supplemental Figure 5A). Higher ATP levels were not caused by rapid intercellular transport of ATP mediated by L-EV, requiring 24 hours to deliver efficacy (Supplemental Figures 5B and 5C). iCMs treated with L-EVs demonstrated

**CENTRAL ILLUSTRATION** Mesenchymal Stem Cell-Derived Extracellular Vesicle-Mediated Mitochondrial Transfer Mitigates Doxorubicin Injury in Patient-Specific Induced Cardiomyocytes



O'Brien, C.G. et al. J Am Coll Cardiol CardioOnc. 2021;3(3):428-440.

Large mesenchymal stem cell extracellular vesicles (L-EVs) transit to and fuse with cardiomyocytes resulting in preserved mitochondrial function, augmentation of ATP production and Peroxisome proliferator-activated receptor-gamma coactivator 1 (PGC-1) alpha transcription, mitigation of ROS production, and suppression of apoptosis. **Up arrows** indicate increased apoptosis; **down arrows** indicate inhibition of apoptosis; and **circular arrows** indicate increased production of a given molecule.

preserved mitochondria biogenesis. Peroxisome proliferator-activated receptor-gamma coactivator-1 alpha expression was greater in iCMs treated with L-EVs than in DOX-injured and uninjured control

subjects ( $P = 0.002$  and  $P = 0.06$ , respectively) (Figure 6C). Finally, we tested whether inhibition of mitochondrial function with MPP<sup>+</sup> (an irreversible inhibitor of mitochondrial function [19]) attenuated

the therapeutic effect of L-EVs. L-EVs incubated in MPP<sup>+</sup> demonstrated loss of mitochondrial viability (Supplemental Figure 4A) and an attenuated therapeutic effect on iCM viability ( $P < 0.001$ ) (Figure 6D), supporting the hypothesis that EV-mediated mitochondrial transfer plays a central role in the ability of MSCs to mitigate myocardial DOX toxicity. Further supporting our hypothesis, RBC-derived L-EVs, which lack mitochondria (Supplemental Figure 7), show no therapeutic benefit.

#### TRIAL TREATMENT ASSIGNMENT AND OUTCOMES.

At the completion of the SENECA trial, we were unblinded to the trial results. In total, 2 of our patients were randomized to placebo and 1 to treatment with allogeneic MSCs. Although low sample size precluded statistical comparisons, the MSC-treated patient demonstrated improved myocardial function and remodeling. Outcomes are summarized in the Table and Supplemental Figure 8. In the SENECA trial, MSC-treated patients demonstrated statistically nonsignificant tendency toward higher ejection fraction, improved global longitudinal strain, reduced myocardial scar burden, and longer 6-minute walk times. MLHFQ scores demonstrated a progressive statistically significant improvement ( $-1.76$  every 6 months;  $P = 0.038$ ) (25).

#### DISCUSSION

Herein, we demonstrate that patient-specific iCMs can be used to conduct an in vitro clinical trial. In this study, we made several novel observations: 1) L-EVs contain viable mitochondria; 2) mitochondrial transfer reversed DOX toxicity in human cardiomyocytes (Central Illustration); and 3) L-EVs can be isolated by a novel technique. Transfer of mitochondria rich L-EVs was associated with improved metrics of iCM function, including improved calcium flux and recovery, stronger contractility, and enhanced viability. Consistent with prior studies of mitochondrial transfer (20), we exhibited that the iCMs receiving exogenous mitochondria demonstrated augmented mitochondrial biogenesis and function. Improved mitochondrial stability may have a direct role in preventing cardiomyocyte apoptosis as increased ATP levels inhibit autophagic flux (26).

One of the primary challenges in deciphering the mechanisms behind stem cell-based therapy in vivo is the rapid rejection of transplanted cells. Here, we demonstrated that MSCs have the ability to rapidly interact with cardiomyocytes via a paracrine mechanism. Furthermore, our observations that MSCs reduced ROS and augmented mitochondrial function imply that the MSCs mitigate progressive

mitochondrial dysfunction and subsequent cardiomyocyte apoptosis, a well-described mechanism of myocardial injury in AIC (4,9). Intercellular transfer of mitochondria is an emerging field of scientific inquiry. Transferred mitochondria are known to undergo fusion with the mitochondria of the recipient cells and play a central role in mitochondrial homeostasis (27).

As SENECA was a phase I trial, caution must be taken when interpreting clinical outcomes. Consistent with previous cell-therapy trials (28), positive tendencies were seen in surrogate markers of cardiovascular performance, whereas imaging studies failed to show statistically significant improvements in ejection fraction and scar. Although MSCs do not appear to lead to myocardial regeneration, our results suggest that MSCs could improve cellular energetics. Recent trials (29) have shown that treating the side effects of chronic myocardial oxidative stress can lead to improved heart failure outcomes. The results herein suggest a mechanism by which MSC therapy could improve cardiovascular performance, and may represent an opportunity for development of cell-free therapy. Identification of such mechanisms implies that myocardial salvage as opposed to regeneration could be the focus of future trial work. Adequate assessment of the reparative changes carries important considerations for trial patient selection, outcome metrics, and patient-physician expectations.

**STUDY LIMITATIONS.** We made several observations that carry implications for the clinical translation of MSCs. MSCs beyond passage 4 produced fewer mitochondria containing L-EVs than younger MSCs (Supplemental Figure 9A), suggesting that fresh MSCs have greater therapeutic potential. Furthermore, L-EVs showed therapeutic benefit in a narrow range of DOX exposure. In a 7-day 0.1- $\mu\text{mol/L}$  DOX exposure assay, L-EVs continued to demonstrate therapeutic efficacy, but the effect was lost when DOX was increased to 0.5  $\mu\text{mol/L}$  (Supplemental Figure 9C). iCMs treated with 10  $\mu\text{mol/L}$  DOX showed no improvement in viability (Supplemental Figure 9B). Similarly, L-EVs added simultaneously with 1  $\mu\text{mol/L}$  DOX had no therapeutic effect (Supplemental Figure 9B). iCMs demonstrate a narrow therapeutic window, and L-EVs may lose efficacy when exposed to DOX. Last, our in vitro iCM results demonstrated that L-EVs mitigate immediate DOX toxicity, which may not translate to efficacy in humans who commonly present with chronic heart failure caused by AIC months to years after treatment. An important caveat to this limitation is that DOX-injured myocardium demonstrates long standing maladaptive

changes stemming from impaired mitochondrial function and biogenesis (30). Mitochondrial transfer could reverse such changes, possibly preventing progressive myocardial dysfunction (31).

## CONCLUSIONS

iPSCs are an invaluable tool for modeling human disease. Our findings suggest an expanded role for iPSC modeling in predicting trial outcomes and evaluating therapeutic mechanisms. Such insights could facilitate therapeutic candidate selection, trial design, and biospecimen collection prior to trial initiation.

**ACKNOWLEDGMENTS** The authors would like to recognize the Cell Sciences Imaging Facility and Shared FACS Facility. They would also like to thank Lisa Nichols for her significant intellectual contribution.

## FUNDING SUPPORT AND AUTHOR DISCLOSURES

Funding for this project was provided by the F-32 Ruth L Kirschstein National Research Service Award and the K-24 Midcareer Investigator Award in Patient Oriented Research from the National Institutes of Health (NIH); and by the Cardiovascular Cell Therapy Research Network (CCTRN) via the UM1 award entitled Regional Clinical Centers for the Cardiovascular Cell Therapy Research Network, University of Texas Health Science Center. The Cardiac Cell Therapy Research Network provided support under the cooperative NIH-sponsored 5UM1HL11345604, 5UM1HL087318-0, and K24HL130553 (all to Dr Yang). Additional project support was provided by an NIH ROO grant (DK111916), Jacob Churg Foundation, McCormick and Gabilan Award, and NIH P30 grant (DK116074) (all to Dr Svensson); NIH F-32 Award (5F32HL139046-02 to Dr O'Brien); and American Heart Association (18CDA34070040 to Dr Wahlquist, 18POST34080005 to Dr Jung, and 20POST35120540 to Dr Ikeda). Dr Gee is a member of the SENECA trial team. Dr Witteles is an associate editor of *JACC: CardioOncology*. Dr Demirci is a founder of and has an

equity interest in DxNow Inc, a company that is developing microfluidic IVF tools and imaging technologies; Koek Biotech, a company that is developing microfluidic technologies for clinical solutions; Levitas Inc, a company focusing on developing microfluidic sorters using magnetic levitation; and Hillel Inc, a company bringing microfluidic cell phone tools to home settings; these interests were viewed and managed in accordance with the conflict of interest policies. Dr Yang is a consultant for Terumo Corporation. All other authors have reported that they have no relationships relevant to the contents of this paper to disclose.

**ADDRESS FOR CORRESPONDENCE:** Dr Phillip C. Yang, Division of Cardiovascular Medicine, Department of Medicine, Stanford University, 240 Pasteur Drive, BMI 3053, Stanford, California 94304, USA. E-mail: [phillip@stanford.edu](mailto:phillip@stanford.edu). Twitter: [@coobrien](https://twitter.com/coobrien).

## PERSPECTIVES

**COMPETENCY IN MEDICAL KNOWLEDGE:** Mitochondrial injury and dysfunction play a central role in AIC. Restoring mitochondrial function may improve myocardial function and viability, a potentially valuable therapeutic avenue in AIC. EV-mediated mitochondrial transfer offers a cell-free technique by which mitochondrial donation can be achieved in target myocardium and possibly reverse doxorubicin injury.

**TRANSLATIONAL OUTLOOK:** Future studies should determine whether EV-mediated mitochondrial transfer can mitigate AIC in vivo. Further testing in chronic in vivo models of AIC would be valuable because chronic cardiomyopathy models hold greater translational value to humans. In depth analysis of cardiovascular performance could prove illuminating because rejuvenation of cellular function may prove physiologically significant despite an absence of myocardial regeneration or improvement in ejection fraction.

## REFERENCES

1. Fornaro A, Olivetto I, Rigacci L, et al. Comparison of long-term outcome in anthracycline-related versus idiopathic dilated cardiomyopathy: a single centre experience. *Eur J Heart Fail*. 2018;20:898-906.
2. Felker GM, Thompson RE, Hare JM, et al. Underlying causes and long-term survival in patients with initially unexplained cardiomyopathy. *N Engl J Med*. 2000;342:1077-1084.
3. Patel KJ, Trédan O, Tannock IF. Distribution of the anticancer drugs doxorubicin, mitoxantrone and topotecan in tumors and normal tissues. *Cancer Chemother Pharmacol*. 2013;72:127-138.
4. Takemura G, Fujiwara H. Doxorubicin-induced cardiomyopathy. From the cardiotoxic mechanisms to management. *Prog Cardiovasc Dis*. 2007;49:330-352.
5. Keizer HG, Pinedo HM, Schuurhuis GJ, Joenje H. Doxorubicin (adriamycin): a critical review of free radical-dependent mechanisms of cytotoxicity. *Pharmacol Ther*. 1990;47(2):219-231.
6. Hasinoff BB, Herman EH. Dextrazoxane: how it works in cardiac and tumor cells. Is it a prodrug or is it a drug? *Cardiovasc Toxicol*. 2007;7:140-144.
7. Vejpongsa P, Yeh ETH. Topoisomerase 2 $\beta$ : a promising molecular target for primary prevention of anthracycline-induced cardiotoxicity. *Clin Pharmacol Ther*. 2014;95:45-52.
8. Liu J, Mao W, Ding B, Liang C-S. ERKs/p53 signal transduction pathway is involved in doxorubicin-induced apoptosis in H9c2 cells and cardiomyocytes. *AJP Hear Circ Physiol*. 2008;295(5):H1956-H1965.
9. Burridge PW, Li YF, Matsa E, et al. Human induced pluripotent stem cell-derived cardiomyocytes recapitulate the predilection of breast cancer patients to doxorubicin-induced cardiotoxicity. *Nat Med*. 2016;22:547-556.
10. Lee AS, Inayathullah M, Lijkwan MA, et al. Prolonged survival of transplanted stem cells after ischaemic injury via the slow release of pro-survival peptides from a collagen matrix. *Nat Biomed Eng*. 2018;2:104-113.
11. Garbade J, Dhein S, Lipinski C, et al. Bone marrow-derived stem cells attenuate impaired contractility and enhance capillary density in a rabbit model of doxorubicin-induced failing hearts. *J Card Surg*. 2009;24(5):591-599. <https://doi.org/10.1111/j.1540-8191.2009.00844.x>
12. Yu Q, Li Q, Na R, et al. Impact of repeated intravenous bone marrow mesenchymal stem cells infusion on myocardial collagen network remodeling in a rat model of doxorubicin-induced dilated cardiomyopathy. *Mol Cell Biochem*. 2014;387(1-2):

- 279-285. <https://doi.org/10.1007/s11010-013-1894-1>
13. Gorji SM, Malekshah AAK, Hashemi-Soteh MB, Rafei A, Parivar K, Aghdami N. Effect of mesenchymal stem cells on doxorubicin-induced fibrosis. *Cell J*. 2012;14(2):142-151.
  14. Zhang Y, Yu Z, Jiang D, et al. iPSC-MSCs with high intrinsic MIRO1 and sensitivity to TNF- $\alpha$  yield efficacious mitochondrial transfer to rescue anthracycline-induced cardiomyopathy. *Stem Cell Reports*. 2016;7(4):749-763. <https://doi.org/10.1016/j.stemcr.2016.08.009>
  15. Churko JM, Burridge PW, Wu JC. Generation of human iPSCs from human peripheral blood mononuclear cells using non-integrative sendai virus in chemically defined conditions. *Methods Mol Biol*. 2013;1036:81-88. [https://doi.org/10.1007/978-1-62703-511-8\\_7](https://doi.org/10.1007/978-1-62703-511-8_7)
  16. Wang Y, Zhang L, Li Y, et al. Exosomes/microvesicles from induced pluripotent stem cells deliver cardioprotective miRNAs and prevent cardiomyocyte apoptosis in the ischemic myocardium. *Int J Cardiol*. 2015;192:61-69.
  17. Liu F, Vermesh O, Mani V, et al. The exosome total isolation chip. *ACS Nano*. 2017;11(11):10712-10723. <https://doi.org/10.1021/acsnano.7b04878>
  18. Santoso MR, Ikeda G, Tada Y, et al. Exosomes from induced pluripotent stem cell-derived cardiomyocytes promote autophagy for myocardial repair. *J Am Heart Assoc*. 2020;9:e014345.
  19. Cleeter MWJ, Cooper JM, Schapira AHV. Irreversible inhibition of mitochondrial complex I by 1-methyl-4-phenylpyridinium: evidence for free radical involvement. *J Neurochem*. 1992;58:786-789.
  20. Ikeda G, Santoso MR, Tada Y, et al. Mitochondria-rich extracellular vesicles from autologous stem cell-derived cardiomyocytes restore energetics of ischemic myocardium. *J Am Coll Cardiol*. 2021;77:1073-1088.
  21. Swenson CE, Bolcsak LE, Batist G, et al. Pharmacokinetics of doxorubicin administered i.v. as Myocet (TLC D-99; liposome-encapsulated doxorubicin citrate) compared with conventional doxorubicin when given in combination with cyclophosphamide in patients with metastatic breast cancer. *Anticancer Drugs*. 2003;14:239-246.
  22. Bramwell VHC, Morris D, Ernst DS, et al. Safety and efficacy of the multidrug-resistance inhibitor biricodar (VX-710) with concurrent doxorubicin in patients with anthracycline-resistant advanced soft tissue sarcoma. *Clin Cancer Res*. 2002;8:383-393.
  23. Haraszti RA, Didiot MC, Sapp E, et al. High-resolution proteomic and lipidomic analysis of exosomes and microvesicles from different cell sources. *J Extracell Vesicles*. 2016;5:32570. <https://doi.org/10.3402/jev.v5.32570>
  24. Ikeda G, Santoso M, Tada Y, et al. Mitochondria containing extracellular vesicles from autologous induced pluripotent stem cell derived cardiomyocytes restore bioenergetics in ischemic myocardium. *J Am Coll Cardiol*. 2021;77(8):1073-1088. <https://doi.org/10.1016/j.jacc.2020.12.060>
  25. Bolli R, Perin E, Willerson J, et al. Allogeneic mesenchymal cell therapy in anthracycline-induced cardiomyopathy heart failure patients. *J Am Coll Cardiol Cardioonc*. 2020;2(4):581-595.
  26. Kobayashi S, Volden P, Timm D, Mao K, Xu X, Liang Q. Transcription factor GATA4 inhibits doxorubicin-induced autophagy and cardiomyocyte death. *J Biol Chem*. 2010;285:793-804.
  27. Ramos ES, Motori E, Brüser C, et al. Mitochondrial fusion is required for regulation of mitochondrial DNA replication. *PLoS Genet*. 2019;15(6):e1008085. <https://doi.org/10.1371/journal.pgen.1008085>
  28. Banerjee MN, Bolli R, Hare JM. Clinical studies of cell therapy in cardiovascular medicine recent developments and future directions. *Circ Res*. 2018;123:266-287.
  29. Armstrong PW, Pieske B, Anstrom KJ, et al. Vericiguat in patients with heart failure and reduced ejection fraction. *N Engl J Med*. 2020;382:1883-1893.
  30. Wallace KB, Sardão VA, Oliveira PJ. Mitochondrial determinants of doxorubicin-induced cardiomyopathy. *Circ Res*. 2020:926-941.
  31. Liu D, Gao Y, Liu J, et al. Intercellular mitochondrial transfer as a means of tissue revitalization. *Signal Transduct Target Ther*. 2021;6(1):65. <https://doi.org/10.1038/s41392-020-00440-z>

---

**KEY WORDS** anthracycline, cardiomyopathy, heart failure

---

**APPENDIX** For an expanded Methods section and supplemental figures, please see the online version of this paper.